MATERIALS CHEMISTRY FRONTIERS

RESEARCH ARTICLE

View Article Online
View Journal | View Issue

Cite this: *Mater. Chem. Front.*, 2022, **6**, 966

Isomeric thermally activated delayed fluorescence emitters based on a quinolino[3,2,1-*de*]acridine-5,9-dione multiple resonance core and carbazole substituent†

Jing-Feng Liu,‡ Sheng-Nan Zou,‡ Xing Chen, Sheng-Yi Yang, You-Jun Yu, Man-Keung Fung, * Zuo-Quan Jiang * and Liang-Sheng Liao

Received 7th December 2021,
Accepted 22nd February 2022

DOI: 10.1039/d1qm01588e

rsc.li/frontiers-materials

The color purity of the pixels is an essential indicator in organic light-emitting diode (OLED) commercial displays. Since the two important parameters of high color purity and efficiency can be achieved simultaneously, multiple resonance thermally activated delayed fluorescence (MR-TADF) emitters have achieved rapid development. Recently, there has been a lot of research work on connecting various donor (D) moieties to the existing MR core, but few studies on how the linking moiety affects the efficiency of MR-TADF emitters. To figure out the influence of substituents on the MR-TADF system, we developed three isomers QAOCz1, QAOCz2, and QAOCz3, which are constructed with the same moieties of 3,11-diphenylquinolino[3,2,1-*de*]acridine-5,9-dione and 9-phenyl-9*H*-carbazole (PhCz) by different site connections. Through reasonable adjustments of the substitution site, the donor–acceptor (D–A) interaction of the isomers gradually weakened and molecular rigidity gradually increased. As a result, their singlet–triplet energy gap (ΔE_{ST}) gradually decreased and their photoluminescence quantum yield (PLQY) gradually rose. QAOCz3 with the weakest D–A interaction successfully achieves a much higher PLQY of 98.9% and a smaller ΔE_{ST} of 0.16 eV. The QAOCz3 based OLED not only realizes the best maximum external quantum efficiency (EQE) of 21.1% but also has the narrowest full-width at half maximum (FWHM) of 40 nm. This work shows that weakening the D–A interaction between the substituents and the MR core by a spacer group is of great significance for the construction of efficient MR-TADF emitters.

1. Introduction

Since the organic light-emitting diodes (OLEDs) were invented by Tang *et al.* in 1987, research on OLEDs has rapidly developed in the past three decades.[1–11] In 2012, the thermally activated delayed fluorescence (TADF) materials were proposed by Adachi's group as the third-generation emitters for OLEDs.[12] In TADF molecular systems, the lowest excited singlet (S_1) and triplet (T_1) states are very close in energy and the small singlet–triplet energy gap (ΔE_{ST}), typically less than 0.4 eV, provides a pathway for non-emissive triplet excitons to emissive singlet excitons *via* reverse intersystem crossing (RISC).[13–28] To achieve high-performance TADF emitters, the common strategy is to separate the highest occupied molecular orbital (HOMO) and the lowest unoccupied molecular orbital (LUMO) into different segments to reduce the electron exchange between them. Therefore, the donor–acceptor (D–A) type design strategy with twisted conformation is formed for this purpose.[13,29–31] However, due to the structural relaxation at S_1 as well as the vibronic coupling between the ground state (S_0) and S_1, large full-width at half maxima (FWHM) (70–100 nm) are usually observed in these emitters, which is a hinderance to the application of OLEDs in commercial displays.

In 2016, Hatakeyama *et al.* introduced a novel design of DABNA series molecules that exhibit high color purity (FWHM ~ 30 nm), in which HOMO/LUMO distributions were realized by the multiple resonance (MR) effects from the oppositely positioned boron and nitrogen atoms in a rigid polycyclic aromatic framework. In this regard, not only the energy gap between S_1 and T_1 but also the vibronic coupling between S_0 and S_1 were minimized for constructing TADF emitters.[32] These kinds of TADF emitters with narrow FWHM

Institute of Functional Nano & Soft Materials (FUNSOM), Jiangsu Key Laboratory for Carbon-Based Functional Materials & Devices, Soochow University, 199 Ren'ai Road, Suzhou, 215123, Jiangsu, P. R. China. E-mail: mkfung@suda.edu.cn, zqjiang@suda.edu.cn

† Electronic supplementary information (ESI) available. CCDC 2026178, 2026179 and 2026181. For ESI and crystallographic data in CIF or other electronic format see DOI: 10.1039/d1qm01588e

‡ Contributed equally.

were thus widely studied and more MR-TADF systems are worth exploring.[33–42] In 2019, our group proposed another example, quinolino[3,2,1-*de*]acridine-5,9-dione (QAO) bearing MR-TADF activity aside from the prevalent B/N system, which consisted of a triphenylamine having two para-disposed carbonyl bridges, and its electroluminescent device achieves the external quantum efficiency (EQE) of 19.4% with the narrow FWHM of 39 nm.[43] From these cores, new MR-TADF emitters can thus be designed by (i) varying the donor patterns, (ii) fusing the conjugated system or (iii) substituting functional groups. Peripheral substitution is the most facile tool to modify the emissive property and deserves systematic study. There are only a handful of examples of utilizing substituents to adjust the QAO MR-TADF system, however.[44–46]

In this work, we developed three cyan isomeric MR-TADF emitters named 3,11-diphenyl-7-(9-phenyl-9*H*-carbazol-3-yl) quinolino[3,2,1-*de*]acridine-5,9-dione (QAOCz1), 7-(4-(9*H*-carbazol-9-yl)phenyl)-3,11-diphenylquinolino[3,2,1-*de*]acridine-5,9-dione (QAOCz2), and 3,11-diphenyl-7-(9-phenyl-9*H*-carbazol-3-yl)quinolino[3,2,1-*de*]acridine-5,9-dione (QAOCz3), which were constructed with the same moieties of acceptor 3,11-diphenylquinolino[3,2,1-*de*]acridine-5,9-dione and donor 9-phenyl-9*H*-carbazole (PhCz) by different site connections. When the carbazole unit is directly connected to the QAO skeleton, QAOCz1 has the strongest D–A interaction, and part of its HOMO is delocalized on the QAO skeleton. By introducing a phenylene bridge to separate the carbazole unit from the QAO skeleton, the D–A interaction of QAOCz2 and QAOCz3 is weakened in which the *meta*-linked QAOCz3 has completely separated HOMO and LUMO. Despite the HOMO–LUMO gradually separating, the FWHM of their electroluminescence (EL) peaks still mainly maintain the nature of the QAO core. We used QAOCz1-, QAOCz2- and QAOCz3-doped films as the emission layers (EMLs), and cyan OLEDs with maximum EQEs of 16.9%, 19.4%, and 21.1% at the EL peaks of 516 (FWHM of 44 nm), 504 (FWHM of 43 nm) and 500 (FWHM of 40 nm) nm were achieved, respectively. The QAOCz3 based device not only achieved the highest maximum EQE of 21.1% but also had the narrowest FWHM of 40 nm. This work shows that the modification of the connection pattern between the substituents and the MR core can also adjust the performance of MR-TADF emitters.

2. Results and discussion

2.1 Synthesis

The synthetic routes for QAOCz1, QAOCz2, and QAOCz3 are summarized in Scheme 1. All compounds were synthesized in six steps from the commercially available starting material 2,5-dibromo-1,3-dimethylbenzene. Above all, precursor dimethyl 2,5-dibromoisophthalate (1) was prepared using a previously reported synthetic procedure.[43] The second step involves the copper-catalyzed C–N coupling between the precursor 1 and di([1,1′-biphenyl]-4-yl)amine, which proceeded smoothly at 142 °C to afford dimethyl 5-bromo-2-(di([1,1′-biphenyl]-4-yl)amino)isophthalate (2) in 84% yield. Furthermore,

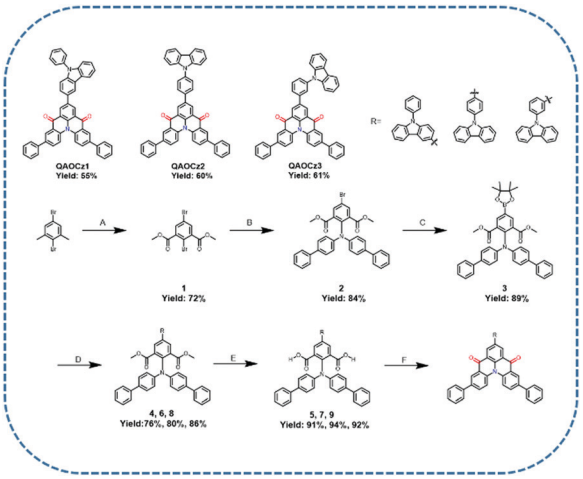

Scheme 1 The synthetic routes of QAOCz1, QAOCz2, and QAOCz3.

dimethyl 2-(di([1,1′-biphenyl]-4-yl)amino)-5-(4,4,5,5-tetramethyl-1,3,2-dioxaborolan-2-yl)isophthalate (3) was prepared from the intermediate 2 and bis(pinacolato)diboron in 89% yield. Next, we introduced a 9-phenyl-9*H*-carbazole unit to obtain the precursor 4, 6, and 8 by Suzuki–Miyaura coupling, and they were smoothly converted into carboxylic acid in the presence of NaOH. Gratifyingly, we obtained the final products QAOCz1, QAOCz2, and QAOCz3 in the yields of 55%, 60%, and 61% by Friedel–Crafts acylation, respectively. In addition to the NMR, mass spectra, and elemental analyses (Fig. S1–S19, ESI†), the key evidence for the formation of the three final compounds was obtained from the single-crystal X-ray diffraction analysis (XRD).

2.2 Single crystals

The single crystals of QAOCz1, QAOCz2, and QAOCz3 were formed by slow diffusion in a mixture of $CHCl_3$ and THF at room temperature (Tables S1–S3, ESI†), then their exact geometries were confirmed by XRD (Fig. 1). Generally, the crystal systems of the three fluorophores are monoclinic lattices, and the QAO skeleton presents helical and nonplanar structures in the three compounds. The repulsion between two hydrogen atoms results in the interplanar angle of 36.75°, 37.30°, and 36.08° between the two benzene rings under the QAO core. For QAOCz1, the carbazole unit is directly connected to the QAO skeleton which forms the strongest D–A interaction and makes the emission wavelength of QAOCz1 longer than that of the other two isomers. After inserting a benzene ring between the carbazole moiety and the QAO skeleton to impede the direct conjugation, the D–A interaction of QAOCz2 and QAOCz3 was weakened. The resulting large dihedral angles of the phenylene bridge and terminal carbazole (58.28° for QAOCz2 and 55.85° for QAOCz3) are beneficial for forming the twisted confirmation at the excited state and inducing effective charge transfer (CT) along with the HOMO and LUMO separation. As compared with QAOCz2, the D–A interaction of QAOCz3 is the weakest by adjusting the substitution site to the *meta*-position.

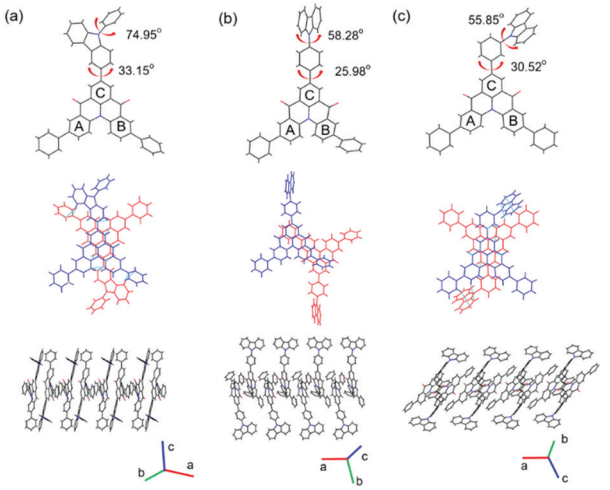

Fig. 1 The single crystals of QAOCz1 (a), QAOCz2 (b), and QAOCz3 (c) obtained by X-ray crystallographic analysis.

The arrangement of the three molecules in the crystalline structure exhibits a head-to-tail packing of the QAO skeleton (Fig. S20, ESI†), and strong intermolecular π–π stacking interactions between the QAO skeletons have been observed (3.256 Å for QAOCz1, 3.314 Å for QAOCz2, 3.365 Å for QAOCz3). Interestingly, the situation is further complicated by the *J*-aggregate with some lateral slippage between the QAO skeleton, which is ascribed to the intramolecular and intermolecular interactions, resulting in the unification of high luminous efficiency and high carrier mobility. Besides, multiple weaker interactions of C–H···C–H, C–H···O, O···C–H, and C–H···π were found in the unit cell, which were associated with different monomers assembling into the 3D structure. Moreover, these weak interactions can strengthen the molecular conformation and at the same time restrict the intramolecular motions and vibrations, which are advantageous to maintain high photoluminescence quantum yields (PLQYs).

2.3 Theoretical simulations

The FMO distributions of the three molecules were calculated based on the single-crystal geometry by density functional theory (DFT) and time-dependent DFT (TD-DFT) calculations. As shown in Fig. 2 and Table S4 (ESI†), due to different degrees of D–A interaction, the three isomers achieve different FMO distributions. The FMOs of QAOCz1 resemble the reported MR effect induced HOMO–LUMO distribution though part of its HOMO electron cloud extends to the carbazole unit. Then, the interaction between D–A was weakened as the phenylene ring was embedded, and the MR effect induced HOMO–LUMO distribution disappeared following the HOMO being completely delocalized to the donor unit. QAOCz2 adopted a twisted conformation of the D–A fragment; meanwhile, its FMO presents a pretty small overlap of HOMO–LUMO. For QAOCz3, its HOMO was completely delocalized at the PhCz skeleton while the LUMO was mainly distributed on the QAO scaffold as the D–A interaction weakened further, which presents a perfect

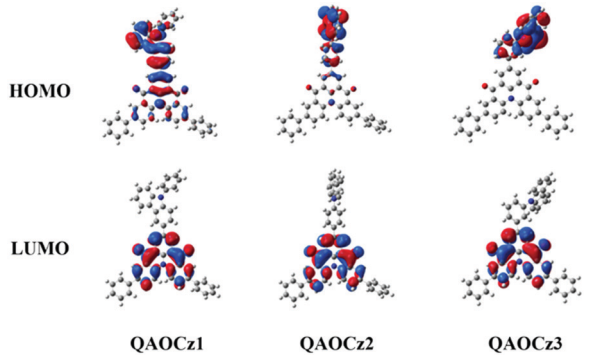

Fig. 2 The molecular structures and HOMO/LUMO distributions of the compounds.

combination of twisted D–A structure and MR skeleton, reflecting that QAOCz3 is allowed RISC at ambient temperatures and the best utilization of triplet excitons. According to the estimated S_1 and T_1 energy levels, the ΔE_{ST}s of QAOCz1, QAOCz2, and QAOCz3 are found to be 0.39, 0.26, and 0.16 eV, respectively, which show a decreasing trend. The calculated HOMO levels are higher than that of the parent molecule QAO, while the LUMO energy level displays a slight change compared with QAO, indicating that the emission will redshift relative to the QAO core. Simulated oscillator strengths (*f*) progressively decrease when the flatness of the isomers is gradually interrupted, which reveals that the electron exchange energy of the three molecules with negative correlation to the rate of radiation transition, and this relationship requires us to balance the two factors to achieve maximum efficiency.

2.4 Photophysical properties

UV-Vis absorption and photoluminescence (PL) spectra of QAOCz1, QAOCz2, and QAOCz3 measured in dilute toluene (10^{-5} mol L^{-1}) solution are shown in Fig. 3 and Table 1. The three isomers all show two major absorption bands; the strong absorption band below 400 nm can be assigned to the π–π* and n–π* transitions of the conjugated skeleton, and the longer

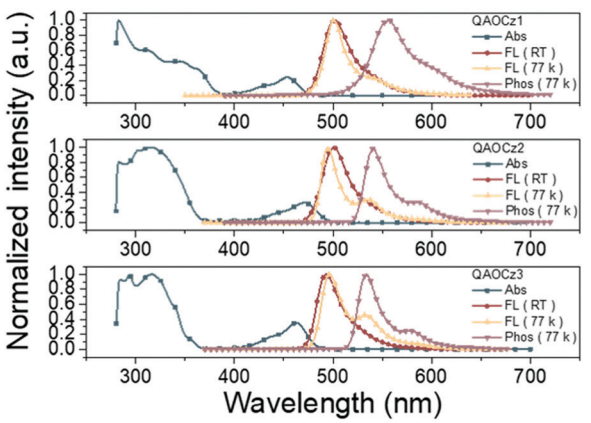

Fig. 3 UV/Vis absorption, fluorescence (298 K), fluorescence (77 K) and phosphorescence (77 K) spectra of QAOCz1, QAOCz2, and QAOCz3 in toluene.

Table 1 Photophysical properties of QAOCz1, QAOCz2, and QAOCz3

Compounds	λ_{abs}[a] (nm)	λ_{em}[a] (nm)	FWHM[a] (nm)	Stokes shift[b] (cm^{-1})	S_1[c] (eV)	T_1[c] (eV)	ΔE_{ST}[c] (eV)
QAOCz1	454	502	34	2106	2.56	2.30	0.26
QAOCz2	471	500	29	1231	2.56	2.38	0.18
QAOCz3	462	492	29	1319	2.55	2.39	0.16

[a] In toluene (10^{-5} M) solution at 298 K. [b] Calculated from the outset of UV absorption and fluorescence spectra in toluene solution (10^{-5} M) at 298 K. [c] Calculated from the outset of fluorescence and phosphorescence spectra in toluene solution (10^{-5} M) at 77 K.

wavelength absorption bands could be originated from the HOMO–LUMO induced intramolecular charge transfer (ICT) transitions. The Stokes shifts of the three emitters are small as expected after the introduction of the PhCz unit, this reflecting that singlet emission regulation and the rigidity enforced by the QAO skeleton well hinder the non-radiative channeling of excitation energy. All three compounds exhibit cyan emission bands with fluorescence spectra peaked at 501, 500, and 495 nm for QAOCz1, QAOCz2, and QAOCz3, respectively, showing a slight blue shift as the D–A interaction is weakened from QAOCz 1 to QAOCz3. Notably, their FWHMs are all narrow: 34 nm for QAOCz1, 29 nm for QAOCz2, and 29 nm for QAOCz3, respectively. We suppose that the wider spectrum of QAOCz1 is associated with its spread FMO distribution. Based on the onsets of fluorescence and phosphorescence spectra in 77 K toluene, the ΔE_{ST} values of the three emitters were calculated to be 0.26, 0.18, and 0.16 eV, respectively. The diminishing trend of the ΔE_{ST} from QAOCz1 to QAOCz3 agrees well with the theoretical results and confirms the feasibility of adjusting the D–A interaction to achieve ΔE_{ST} regulation of MR-TADF emitters. To further figure out the excitation transition feature, we have tested the PL spectra of the three compounds in different solvents at room temperature. As shown in Fig. S21 (ESI†), an obvious solvatochromic effect can be observed for the three emitters with the polarity of the solvent increasing from nonpolar hexane to the highest polar acetone. In particular with the increase of environmental polarity, the spectra gradually show characterless variations. These results further confirm the three emitters as strong transitions of ICT states.

The solid-state photoluminescence behaviors of QAOCz1, QAOCz2, and QAOCz3 were also investigated in films (Table S5, ESI†). Fig. S22 (ESI†) shows the PL spectra of the films doped with 5 wt% emitters in 4,4′-bis(9*H*-carbazol-9-yl)biphenyl (CBP), and a low doping concentration was chosen to prevent the aggregation of the emitters. Although the PhCz unit and the QAO framework are connected through different modes, the three emitters all show a narrow spectral shape in the doped films as shown previously. Besides, the absolute PLQYs of the three doped films with 5 wt% CBP were measured to be 86.1% for QAOCz1, 86.8% for QAOCz2, and 98.9% for QAOCz3, respectively. Due to the increase in rigidity, the PLQYs of the three isomers all showed an upward trend. To further verify the TADF character of QAOCz1, QAOCz2, and QAOCz3, we explored their transient photoluminescence (PL) decays in dopant films. As shown in Fig. S23 (ESI†), the decay lifetimes of the three emitters were 115.7 μs for QAOCz1, 16.4 μs for QAOCz2, and 21.5 μs for QAOCz3, respectively, indicative of obvious TADF nature. Fig. S24 (ESI†) shows the PL spectra of the three compounds in non-doped films, different from the QAO, they retain their narrow spectral shape and avoid excimer formation.

2.5 Thermal analysis and electrochemical behaviors

To explore the thermal stabilities of QAOCz1, QAOCz2, and QAOCz3, the thermal decomposition temperature (T_d) was measured by thermogravimetric analysis (TGA) under a nitrogen atmosphere. The experimental results are shown in Fig. S25 (ESI†) and the detailed data are listed in Table S6 (ESI†). The T_d (5 wt% weight loss) was found to be 459, 460, and 469 °C for QAOCz1, QAOCz2, and QAOCz3, respectively. In addition, to select the suitable functional layer in the device, the electrochemical behaviors of three molecules were investigated by cyclic voltammetry (CV) in dry *N*,*N*-dimethylformamide (DMF) using the internal reference of ferrocene. As shown in Fig. S26 and Table S6 (ESI†), all isomers show similar HOMO energy levels (−5.47, −5.54, and −5.47 eV), which are very close to the HOMO energy level of parent PhCz (−5.51 eV) and significantly higher than the original QAO backbone (−5.94 eV). On the other hand, based on their HOMO energy levels and the optical band gaps, the LUMO energy levels were calculated to be −3.02, −3.06, and −2.96 eV for QAOCz1, QAOCz2, and QAOCz3, respectively.

2.6 Electroluminescence properties

To investigate the electroluminescence (EL) properties of the three emitters, the devices were fabricated with a structure of indium tin oxide (ITO)/1,4,5,8,9,11-hexaazatriphenylene hexacarbonitrile (HAT-CN, 10 nm)/1,1-bis[4-[*N*, *N*-di(p-tolyl)amino]-phenyl]-cyclohexane (TAPC, 40 nm)/tris(4-carbazolyl-9-ylphenyl)amine (TCTA, 10 nm)/EML (20 nm)/4,6-bis(3,5-di(4yridine-4-yl)phenyl)-2-phenylpyrimidine (TmPyPB, 50 nm)/8-hydroxyquinolinolato lithium (Liq, 2 nm)/Al (100 nm). D1, D2, and D3 represent QAOCz1, QAOCz2, and QAOCz3-based devices, respectively. The EL spectra at the current density of 5 mA cm^{-2} (Fig. S27, ESI†), EL spectra at different applied voltages (Fig. S28, ESI†), power efficiency (PE)–luminance (*L*) characteristics (Fig. S29, ESI†), and current efficiency (CE)–luminance (*L*) characteristics (Fig. S29, ESI†) of OLEDs are shown in the supporting information. The EL spectral intensity increases significantly with increasing voltage, but all spectra are quite stable. Fig. 4a and c show the energy level diagram of the devices and molecular structures of related functional materials, respectively. TAPC and TmPyPB were selected as the hole-transporting layer and the electron-transporting layer, and TCTA was used as an exciton-blocking layer for confining excitons due to its high triplet energy level. For the emitting layer, CBP was chosen as the host and the optimized dopant ratio was 5 wt% for the three emitters. Fig. 4b shows the current density (*J*)–voltage (*V*)–luminance (*L*) characteristics of the OLEDs, and the driving voltage of the emitter-based devices at 6 cd m^{-2} is 3.3 V, which may be attributed to the good carrier

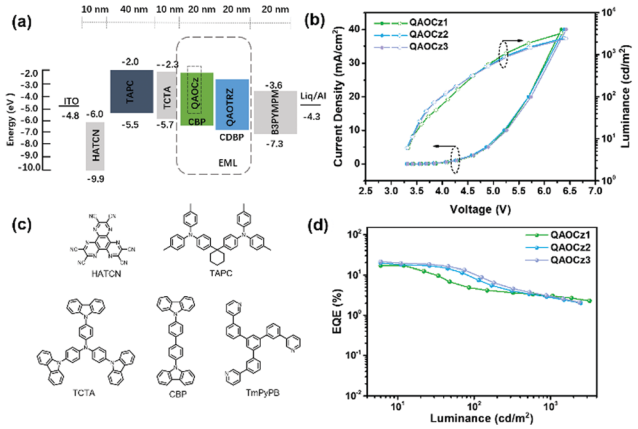

Fig. 4 (a) Energy level diagrams of the devices, (b) *J*–*V*–*L* characteristics and (c) molecular structures of other materials used in these devices, and (d) EQE–luminance characteristics of the QAOCz1, QAOCz2, and QAOCz3-based devices.

Table 2 Summary of the electroluminescence data of QAOCz1, QAOCz2, and QAOCz3-based devices

	λ_{EL}[a] (nm)	FWHM[b] (nm)	V_{on}[c] (V)	CE_{max}[d] (cd A^{-1})	PE_{max}[e] (lm W^{-1})	EQE[f] (%)	CIE[g] (*x*, *y*)	L[h] (cd m^{-2})
QAOCz1	516	44	3.3	60	56.5	16.9	(0.23, 0.66)	11320
QAOCz2	504	43	3.3	60	57.0	19.4	(0.18, 0.62)	7679
QAOCz3	500	40	3.3	60	56.7	21.1	(0.16, 0.57)	6217

[a] EL peak wavelength. [b] Full width at half maximum. [c] Turn-on voltage. [d] Maximum current efficiency. [e] Maximum power efficiency. [f] Maximum external quantum efficiency. [g] CIE measured at the current density of 5 mA cm^{-2}. [h] Maximum luminance.

injection and transportation of the three emitters. Fig. 4b shows the luminance (*L*)–EQE characteristics of the OLEDs. The emission peaks of D1, D2, and D3 are 516, 504, and 500 nm, and the full width at half maximum (FWHM) of the EL spectra are 44, 43, and 40 nm, and the corresponding color coordinates are (0.23, 0.66), (0.18, 0.62) and (0.16, 0.57), respectively (Table 2). And we further judged the color purity of the three molecules using the range-separated hybrid (RSH) functions previously proposed by our group.[47] Based on the calculation equation, the RSHs of D1, D2, and D3 were calculated to be 1.98, 1.96, and 1.98, respectively, which are all close to 1.7, further illustrating that these devices all exhibit good color purity (Table S7, ESI†). The maximum EQE (EQE_{max}) of D1 could reach 16.9%. Furthermore, D2 and D3 exhibit EQE_{max} of 19.4% and 21.1%, respectively. The best performance of QAOCz3 in this series could be attributed to its smallest ΔE_{ST} and highest PLQY, corresponding to the *meta*-linkage between the QAO core and carbazole substituent.

Conclusions

In summary, we have developed three narrowband isomers, namely QAOCz1, QAOCz2, and QAOCz3 based on the QAO core and the PhCz unit. Combining theoretical calculations, photoelectric behavior, and OLED performance, the influence of weakening D–A interaction on these structural isomers was systematically studied. As the D–A interaction of the isomers is gradually weakened, their HOMO and LUMO energy levels are gradually separated, so the ΔE_{ST}s are gradually decreased. And the PLQYs of QAOCz1, QAOCz2, and QAOCz3 gradually increased, which are 86.1%, 86.8%, and 98.9%, respectively. Eventually, OLEDs based on QAOCz1, QAOCz2 and QAOCz3 as the emitters exhibit EQE_{max}s, emission peaks and CIEs (x, y) of 16.9%, 516 nm and (0.23, 0.66), 19.4%, 504 nm and (0.18, 0.62), and 21.1%, 500 nm and (0.16, 0.57), respectively. In addition, although the PhCz unit with weaker electron-donating ability has little effect on color purity, and their EL spectra all exhibit narrow emission, the FWHMs of the three isomers still narrowed slightly with the weakening of the D–A interaction. And the FWHMs of QAOCz1, QAOCz2, and QAOCz3 are 44, 43, and 40 nm respectively. The *meta*-linked QAOCz3 has the weakest D–A interaction and successfully achieves a much higher PLQY and a smaller ΔE_{ST}, and the QAOCz3 based OLED displays the highest maximum EQE and the narrowest FWHM. These results show that the substituent with weak electron-donating ability can well maintain the narrowband emission characteristics of the MR framework. And the method of weakening the D–A interaction between the substituents and the MR skeleton by a spacer group can improve the efficiency while further narrowing the FWHM. Therefore, we proposed an efficient strategy for constructing a MR-TADF emitter with both high efficiency and narrow FWHM.

Conflicts of interest

The authors declare no conflict of interest.

Acknowledgements

The authors acknowledge financial support from the National Natural Science Foundation of China (grant No. 51773141, 51873139, 61961160731, 62175171, and 22175124). This project is also funded by the Suzhou Science and Technology Plan Project (SYG202010). This work is also supported by Suzhou Key Laboratory of Functional Nano & Soft Materials, Collaborative Innovation Center of Suzhou Nano Science & Technology, the 111 Project, and Joint International Research Laboratory of Carbon-Based Functional Materials and Devices.

Notes and references

1 C. W. Tang and S. A. VanSlyke, Organic electroluminescent diodes, *Appl. Phys. Lett.*, 1987, **51**, 913–915.
2 J. J. Kido, M. Kimura and K. Nagai, Multilayer white light-emitting organic electroluminescent device, *Science*, 1995, 1332–1334.
3 M. A. Baldo, D. F. O'Brien, Y. You, A. Shoustikov, S. Sibley, M. E. Thompson and S. R. Forrest, Highly efficient

phosphorescent emission from organic electroluminescent devices, *Nature*, 1998, **395**, 151–154.
4 C. Adachi, M. A. Baldo, M. E. Thompson and S. R. Forrest, Nearly 100% internal phosphorescence efficiency in an organic light-emitting device, *J. Appl. Phys.*, 2001, **90**, 5048.
5 M. Segal, M. A. Baldo, R. J. Holmes, S. R. Forrest and Z. G. Soos, Excitonic singlet-triplet ratios in molecular and polymeric organic materials, *Phys. Rev. B: Condens. Matter Mater. Phys.*, 2003, **68**, 075211.
6 S. W. Wen, M. T. Lee and C. H. Chen, Recent development of blue fluorescent OLED materials and devices, *J. Disp. Technol.*, 2005, **1**, 90–99.
7 H.-C. Li, X. Tang, S.-Y. Yang, Y.-K. Qu, Z.-Q. Jiang and L.-S. Liao, Spatial donor/acceptor architecture for intramolecular charge-transfer emitter, *Chin. Chem. Lett.*, 2021, **32**, 1245–1248.
8 J. A. Rogers, T. Someya and Y. G. Huang, Materials and mechanics for stretchable electronics, *Science*, 2010, 1603–1607.
9 Y. Xu, X. Liang, X. Zhou, P. Yuan, J. Zhou, C. Wang, B. Li, D. Hu, X. Qiao, X. Jiang, L. Liu, S. J. Su, D. Ma and Y. Ma, Highly efficient blue fluorescent OLEDs based on upper level triplet–singlet intersystem crossing, *Adv. Mater.*, 2019, **31**, 1807388.
10 L. Y. Hsu, D. G. Chen, S. H. Liu, T. Y. Chiu, C. H. Chang, A. K. Jen, P. T. Chou and Y. Chi, Roles of ancillary chelates and overall charges of bis-tridentate Ir(III) phosphors for OLED applications, *ACS Appl. Mater. Interfaces*, 2020, **12**, 1084–1093.
11 Y. C. Wei, S. F. Wang, Y. Hu, L. S. Liao, D. G. Chen, K. H. Chang, C. W. Wang, S. H. Liu, W. H. Chan, J. L. Liao, W. Y. Hung, T. H. Wang, P. T. Chen, H. F. Hsu, Y. Chi and P. T. Chou, Overcoming the energy gap law in near-infrared OLEDs by exciton–vibration decoupling, *Nat. Photonics*, 2020, **14**, 570–577.
12 H. Uoyama, K. Goushi, K. Shizu, H. Nomura and C. Adachi, Highly efficient organic light-emitting diodes from delayed fluorescence, *Nature*, 2012, **492**, 234–238.
13 Q. Zhang, J. Li, K. Shizu, S. Huang, S. Hirata, H. Miyazaki and C. Adachi, Design of efficient thermally activated delayed fluorescence materials for pure blue organic light emitting diodes, *J. Am. Chem. Soc.*, 2012, **134**, 14706–14709.
14 F. B. Dias, K. N. Bourdakos, V. Jankus, K. C. Moss, K. T. Kamtekar, V. Bhalla, J. Santos, M. R. Bryce and A. P. Monkman, Triplet harvesting with 100% efficiency by way of thermally activated delayed fluorescence in charge transfer OLED emitters, *Adv. Mater.*, 2013, **25**, 3707–3714.
15 K. Suzuki, S. Kubo, K. Shizu, T. Fukushima, A. Wakamiya, Y. Murata, C. Adachi and H. Kaji, Triarylboron-based fluorescent organic light-emitting diodes with external quantum efficiencies exceeding 20%, *Angew. Chem., Int. Ed.*, 2015, **54**, 15231–15235.
16 T. A. Lin, T. Chatterjee, W. L. Tsai, W. K. Lee, M. J. Wu, M. Jiao, K. C. Pan, C. L. Yi, C. L. Chung, K. T. Wong and C. C. Wu, Sky-blue organic light emitting diode with 37% external quantum efficiency using thermally activated delayed fluorescence from spiroacridine-triazine hybrid, *Adv. Mater.*, 2016, **28**, 6976–6983.
17 C. Han, C. Duan, W. Yang, M. Xie and H. Xu, Allochroic thermally activated delayed fluorescence diodes through field-induced solvatochromic effect, *Sci. Adv.*, 2017, **3**, 1700904.
18 Y. Im, M. Kim, Y. J. Cho, J. A. Seo, K. S. Yook and J. Y. Lee, Molecular design strategy of organic thermally activated delayed fluorescence emitters, *Chem. Mater.*, 2017, **29**, 1946–1963.
19 X. Cai and S. J. Su, Marching toward highly efficient, pure-blue, and stable thermally activated delayed fluorescent organic light-emitting diodes, *Adv. Funct. Mater.*, 2018, **28**, 1802558.
20 Y. Z. Shi, K. Wang, X. Li, G. L. Dai, W. Liu, K. Ke, M. Zhang, S. L. Tao, C. J. Zheng, X. M. Ou and X. H. Zhang, Intermolecular charge-transfer transition emitter showing thermally activated delayed fluorescence for efficient non-doped OLEDs, *Angew. Chem., Int. Ed.*, 2018, **57**, 9480–9484.
21 J. Xue, Q. Liang, R. Wang, J. Hou, W. Li, Q. Peng, Z. Shuai and J. Qiao, Highly efficient thermally activated delayed fluorescence via J-aggregates with strong intermolecular charge transfer, *Adv. Mater.*, 2019, **31**, 1808242.
22 B. Zhao, H. Wang, C. Han, P. Ma, Z. Li, P. Chang and H. Xu, Highly efficient deep-red non-doped diodes based on a T-shape thermally activated delayed fluorescence emitter, *Angew. Chem., Int. Ed.*, 2020, **59**, 19042–19047.
23 X. Tang, L. S. Cui, H. C. Li, A. J. Gillett, F. Auras, Y. K. Qu, C. Zhong, S. T. E. Jones, Z. Q. Jiang, R. H. Friend and L. S. Liao, Highly efficient luminescence from space-confined charge-transfer emitters, *Nat. Mater.*, 2020, **19**, 1332–1338.
24 Z. Cai, X. Wu, H. Liu, J. Guo, D. Yang, D. Ma, Z. Zhao and B. Z. Tang, Realizing record-high electroluminescence efficiency of 31.5% for red thermally activated delayed fluorescence molecules, *Angew. Chem., Int. Ed.*, 2021, **60**, 23635–23640.
25 Q. Xue and G. Xie, Thermally activated delayed fluorescence beyond throughbond Charge transfer for high-performance OLEDs, *Adv. Opt. Mater.*, 2021, **9**, 2002204.
26 P. Xue, X. Wang, W. Wang, J. Zhang, Z. Wang, J. Jin, C. Zheng, P. Li, G. Xie and R. Chen, Solution-Processable Chiral Boron Complexes for Circularly Polarized Red Thermally Activated Delayed Fluorescent Devices, *ACS Appl. Mater. Interfaces*, 2021, **13**, 47826–47834.
27 S. Y. Yang, Y. K. Qu, L. S. Liao, Z. Q. Jiang and S. T. Lee, Research progress of intramolecular π-stacked small molecules for device applications, *Adv. Mater.*, 2021, 2104125.
28 Y. K. Qu, Q. Zheng, J. Fan, L. S. Liao and Z. Q. Jiang, Spiro compounds for organic light-emitting diodes, *Acc. Mater. Res.*, 2021, **2**, 1261–1271.
29 K. Goushi, K. Yoshida, K. Sato and C. Adachi, High reverse intersystem crossing efficiency using an exciplex state and application to organic light-emitting diodes, *Nat. Photonics*, 2012, **6**, 253–258.
30 G. Mehes, H. Nomura, Q. Zhang, T. Nakagawa and C. Adachi, Enhanced electroluminescence efficiency in a

spiro-acridine derivative through thermally activated delayed fluorescence, *Angew. Chem., Int. Ed.*, 2012, **51**, 11311–11315.

31 D. Zhang, X. Song, M. Cai, H. Kaji and L. Duan, Versatile indolocarbazole-isomer derivatives as highly emissive emitters and ideal hosts for thermally activated delayed fluorescent OLEDs with alleviated efficiency roll-off, *Adv. Mater.*, 2018, **30**, 1705406.

32 T. Hatakeyama, K. Shiren, K. Nakajima, S. Nomura, S. Nakatsuka, K. Kinoshita, J. Ni, Y. Ono and T. Ikuta, Ultrapure blue thermally activated delayed fluorescence molecules: efficient HOMO–LUMO separation by the multiple resonance effect, *Adv. Mater.*, 2016, **28**, 2777–2781.

33 S. M. Suresh, E. Duda, D. Hall, Z. Yao, S. Bagnich, A. M. Z. Slawin, H. Bassler, D. Beljonne, M. Buck, Y. Olivier, A. Kohler and E. Zysman-Colman, A deep blue B, N-doped heptacene emitter that shows both thermally activated delayed fluorescence and delayed fluorescence by triplet–triplet annihilation, *J. Am. Chem. Soc.*, 2020, **142**, 6588–6599.

34 P. Jiang, J. Miao, X. Cao, H. Xia, K. Pan, T. Hua, X. Lv, Z. Huang, Y. Zou and C. Yang, Quenching-resistant multiresonance TADF emitter realizes 40% external quantum efficiency in narrowband electroluminescence at high doping level, *Adv. Mater.*, 2022, **34**, 2106954.

35 X. Wu, J. W. Huang, B. K. Su, S. Wang, L. Yuan, W. Q. Zheng, H. Zhang, Y. X. Zheng, W. Zhu and P. T. Chou, Fabrication of circularly polarized MR-TADF emitters with asymmetrical peripheral-lock enhancing helical B/N-doped nanographenes, *Adv. Mater.*, 2022, **34**, 2105080.

36 X. Wu, B. K. Su, D. G. Chen, D. Liu, C. C. Wu, Z. X. Huang, T. C. Lin, C. H. Wu, M. Zhu, E. Y. Li, W. Y. Hung, W. Zhu and P. T. Chou, The role of host–guest interactions in organic emitters employing MR-TADF, *Nat. Photonics*, 2021, **15**, 780–786.

37 M. Yang, S. Shikita, H. Min, I. S. Park, H. Shibata, N. Amanokura and T. Yasuda, Wide-range color tuning of narrowband emission in multi-resonance organoboron delayed fluorescence materials through rational imine/amine functionalization, *Angew. Chem., Int. Ed.*, 2021, **60**, 23142–23147.

38 J. Park, J. Lim, J. H. Lee, B. Jang, J. H. Han, S. S. Yoon and J. Y. Lee, Asymmetric blue multiresonance TADF emitters with a narrow emission band, *ACS Appl. Mater. Interfaces*, 2021, **13**, 45798–45805.

39 Y. Liu, X. Xiao, Y. Ran, Z. Bin and J. You, Molecular design of thermally activated delayed fluorescent emitters for narrowband orange–red OLEDs boosted by a cyano-functionalization strategy, *Chem. Sci.*, 2021, **12**, 9408–9412.

40 Y. Xu, Q. Wang, X. Cai, C. Li and Y. Wang, Highly efficient electroluminescence from narrowband green circularly polarized multiple resonance thermally activated delayed fluorescence enantiomers, *Adv. Mater.*, 2021, **33**, 2100652.

41 Y. Zhang, D. Zhang, T. Huang, A. J. Gillett, Y. Liu, D. Hu, L. Cui, Z. Bin, G. Li, J. Wei and L. Duan, Multi-resonance deep-red emitters with shallow potential-energy surfaces to surpass energy-gap law, *Angew. Chem., Int. Ed.*, 2021, **60**, 20498–20503.

42 H. Tanaka, S. Oda, G. Ricci, H. Gotoh, K. Tabata, R. Kawasumi, D. Beljonne, Y. Olivier and T. Hatakeyama, Hypsochromic shift of multiple-resonance-induced thermally activated delayed fluorescence by oxygen atom incorporation, *Angew. Chem., Int. Ed.*, 2021, **60**, 17910–17914.

43 Y. Yuan, X. Tang, X. Y. Du, Y. Hu, Y. J. Yu, Z. Q. Jiang, L. S. Liao and S. T. Lee, The design of fused amine/carbonyl system for efficient thermally activated delayed fluorescence: novel multiple resonance core and electron acceptor, *Adv. Opt. Mater.*, 2019, **7**, 1801536.

44 D. Sun, S. M. Suresh, D. Hall, M. Zhang, C. Si, D. B. Cordes, A. M. Z. Slawin, Y. Olivier, X. Zhang and E. Zysman-Colman, The design of an extended multiple resonance TADF emitter based on a polycyclic amine/carbonyl system, *Mater. Chem. Front.*, 2020, **4**, 2018–2022.

45 S. N. Zou, C. C. Peng, S. Y. Yang, Y. K. Qu, Y. J. Yu, X. Chen, Z. Q. Jiang and L. S. Liao, fully bridged triphenylamine derivatives as color-tunable thermally activated delayed fluorescence emitters, *Org. Lett.*, 2021, **23**, 958–962.

46 F. Huang, K. Wang, Y. Z. Shi, X. C. Fan, X. Zhang, J. Yu, C. S. Lee and X. H. Zhang, Approaching efficient and narrow RGB electroluminescence from D–A-type TADF emitters containing an identical multiple resonance backbone as the acceptor, *ACS Appl. Mater. Interfaces*, 2021, **13**, 36089–36097.

47 A. Khan, X. Tang, C. Zhong, Q. Wang, S. Y. Yang, F. C. Kong, S. Yuan, A. S. D. Sandanayaka, C. Adachi, Z. Q. Jiang and L. S. Liao, Intramolecular-locked high efficiency ultrapure violet-blue (CIE-y <0.046) thermally activated delayed fluorescence emitters exhibiting amplified spontaneous emission, *Adv. Funct. Mater.*, 2021, **31**, 2009488.

